TOPOLOGY DESIGN OF PLATES CONSIDERING DIFFERENT VOLUME CONTROL METHODS

DIEGO E. CAMPEÃO, SEBASTIÁN M. GIUSTI, AND ANTONIO A. NOVOTNY

Abstract.
Purpose. Comparison between two methods of volume control in the context of topological derivative-based structural optimization of Kirchhoff plates.
Methodology. The compliance topology optimization of Kirchhoff plates subjected to volume constraint is considered. In order to impose the volume constraint, two method are presented. The first one is done by means of a linear penalization method. In this case, the penalty parameter is the coefficient of a linear term used to control the amount of material to be removed. The second approach is based on the Augmented Lagrangian method which has both, linear and quadratic terms. The coefficient of the quadratic part controls the Lagrange multiplier update of the linear part. The associated topological sensitivity is used to devise a structural design algorithm based on the topological derivative and a level-set domain representation method. Finally, some numerical experiments are presented allowing for a comparative analysis between the two methods of volume control from a qualitative point of view.
Findings. The linear penalization method does not provide direct control over the required volume fraction. In contrast, through the Augmented Lagrangian method it is possible to specify the final amount of material in the optimized structure.
Originality. A strictly simple topology design algorithm is devised and used in the context of compliance structural optimization of Kirchhoff plates under volume constraint. The proposed computational framework is quite general and can be applied in different engineering problems.
Keywords. Topological derivative, Level-set domain representation, Topology optimization, Kirchhoff plates.
Article type. Research paper.

1. Introduction

The technological progress in the last decades has enabled the design and construction of structural plate elements by using materials with different mechanical properties. In this context, the optimal distribution of these materials in a particular structural element is of paramount importance in many areas such as civil, mechanical, aerospace, biomedical and nuclear engineering. A quite general approach to deal with this kind of problem is based on the relatively new mathematical notion of topological derivative (Sokołowski and Żochowski (1999)). See also the book by Novotny and Sokołowski (2013).

In order to introduce this concept, let us consider a bounded domain $\Omega \subset \mathbb{R}^2$, which is subjected to a non-smooth perturbation confined in a small region $\omega_\varepsilon(\widehat{x}) = \widehat{x} + \varepsilon\omega$ of size ε, as shown in fig. 1. Here, $\widehat{x}$ is an arbitrary point of Ω and ω is a fixed domain of $\mathbb{R}^2$. We introduce a characteristic function associated to the unperturbed domain, namely $\chi = \mathbb{1}_\Omega$. Then, we define a characteristic function associated to the topologically perturbed domain of the form χ_ε. In the present case, the perturbed domain is obtained when a circular hole $\omega_\varepsilon(\widehat{x}) = B_\varepsilon(\widehat{x})$ is introduced inside the domain Ω, where $B_\varepsilon(\widehat{x})$ is used to denote a ball of radius ε and center at $\widehat{x} \in \Omega$. Next, this region is filled by an inclusion with different material property. To describe this feature, we introduce a piecewise constant function γ_ε of the form

$$\gamma_\varepsilon = \gamma_\varepsilon(x) := \begin{cases} 1 & \text{if } x \in \Omega \setminus \overline{B_\varepsilon} \\ \gamma & \text{if } x \in B_\varepsilon \end{cases} , \tag{1}$$

where $\gamma \in \mathbb{R}^+$ is the contrast in the material property. Therefore the characteristic function χ_ε takes the form $\chi_\varepsilon(\widehat{x}) = \mathbb{1}_\Omega - (1-\gamma)\mathbb{1}_{\overline{B_\varepsilon(\widehat{x})}}$. Then, we assume that a given shape functional

$\psi(\chi_\varepsilon(\widehat{x}))$, associated to the topologically perturbed domain, admits the following topological asymptotic expansion

$$\psi(\chi_\varepsilon(\widehat{x})) = \psi(\chi) + f(\varepsilon)\mathcal{T}_\Omega(\widehat{x}) + o(f(\varepsilon)) \,, \tag{2}$$

where $\psi(\chi)$ is the shape functional associated to the original (unperturbed) domain, $f(\varepsilon)$ is a positive function such that $f(\varepsilon) \to 0$, when $\varepsilon \to 0$. The function $\widehat{x} \mapsto \mathcal{T}_\Omega(\widehat{x})$ is called the topological derivative of ψ at $\widehat{x}$. Therefore, this derivative can be seen as a first order correction of $\psi(\chi)$ to approximate $\psi(\chi_\varepsilon(\widehat{x}))$. In fact, the topological derivative measures the sensitivity of a given shape functional with respect to an infinitesimal singular domain perturbation, such as the insertion of holes, inclusions, source-terms or even cracks. This concept has proved to be extremely useful in the treatment of a wide range of problems, namely, topology optimization (Allaire et al. (2005); Amstutz and Andrä (2006); Amstutz and Novotny (2010); Giusti et al. (2010); Amstutz et al. (2012)), inverse analysis (Hintermüller and Laurain (2008); Amstutz et al. (2005); Hintermüller et al. (2012)), image processing (Hintermüller and Laurain (2009); Larrabide et al. (2008)), multi-scale constitutive modeling (Giusti et al. (2009); Amstutz et al. (2010)), fracture mechanics sensitivity analysis (Van Goethem and Novotny (2010)) and damage evolution modeling (Allaire et al. (2011)).

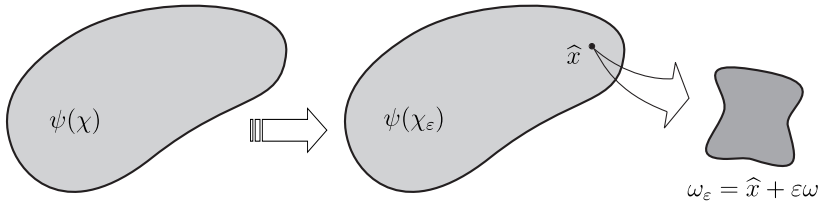

FIGURE 1. The topological derivative concept.

In Novotny et al. (2005) the topological derivative was obtained, through the approach developed in Novotny et al. (2003), for the total potential energy associated to the Kirchhoff plate bending problem, considering as singular perturbation the nucleation of a circular hole. This result was used to devise a hard-kill like topology algorithm and some numerical experiments were presented. More recently, a numerical method to compute the first-order variation of some quantity of interest when an arbitrary-shaped feature is introduced in the plate domain has been proposed in Turevsky et al. (2009). Also, in Bojczuk and Mróz (2009) the topological derivative with respect to the introduction of reinforcements in a plate was presented and discussed in details. In Amstutz (2010) the closed formulas associated to a large class of shape functionals were derived using the approach proposed in Amstutz (2006) and a full mathematical justification for the formula obtained in Novotny et al. (2005) was provided. In addition, the result derived in Novotny et al. (2005) was extended by considering as topological perturbation the nucleation of an infinitesimal circular inclusion instead of a hole. This last result allows to devise a topology design algorithm as proposed in Amstutz and Andrä (2006).

Therefore, as a natural sequence of this research, in this work we propose an optimization algorithm based on the topological derivative and a level-set domain representation for the compliance topology design of Kirchhoff plates, with volume constraint. In particular, we compare two methods of volume control in the context of topological derivative-based structural optimization. The first one is done by means of linear penalization and does not provide direct control over the required volume fraction. In this case, the penalty parameter is the coefficient of a linear term used to control the amount of material to be removed. The second approach is based on the Augmented Lagrangian method which has both, linear and quadratic terms. The coefficient of the quadratic part controls the Lagrange multiplier update of the linear part. Through this last method it is possible to specify the final amount of material in the optimized structure. In order to present the behavior of both approaches, we consider the compliance topology optimization of Kirchhoff plates subjected to volume constraint.

This paper is organized as follows. Section 2 describes the compliance topology optimization problem of Kirchhoff plates subjected to volume constraint. The two methods used to impose the volume constraint are presented in Section 3. The structural design algorithm based on the topological derivative and a level-set domain representation method are outlined in Section 4. A set of numerical experiments is presented in Section 5, allowing for a comparative analysis between the two implemented methods of volume control from a qualitative point of view. The paper ends in Section 6 with some concluding remarks.

2. Problem formulation

The most popular topology optimization problem consists in minimizing the structural compliance for a given amount of material. It can be written as

$$\left\{ \begin{array}{lrcl} \text{Minimize} & \psi(\chi) & = & -\mathcal{J}_\chi(u) \, , \\ \text{Subjected to} & |\Omega| & \leq & V \, , \end{array} \right. \tag{3}$$

where $|\Omega|$ denotes the volume of the domain Ω, V is the required volume at the end of the optimization process and $\psi(\chi)$ is the energy functional associated to the Kirchhoff plate bending problem, which is given by

$$\mathcal{J}_\chi(u) = -\frac{1}{2}\int_\Omega M(u)\cdot\nabla\nabla u - \int_{\Gamma_{N_q}} \overline{q}u + \int_{\Gamma_{N_m}} \overline{m}\partial_n u + \sum_{i=1}^{ns} \overline{Q}_i u(x_i) \, , \tag{4}$$

where $\partial_n(\cdot)$ is used to denote the normal derivative of $(\cdot)$ and u is the deflection function, the solution to the variational problem:

$$\left\{ \begin{array}{l} \text{Find } u \in \mathcal{U}, \text{ such that} \\ -\displaystyle\int_\Omega M(u)\cdot\nabla\nabla\eta = \int_{\Gamma_{N_q}} \overline{q}\eta - \int_{\Gamma_{N_m}} \overline{m}\partial_n\eta - \sum_{i=1}^{ns} \overline{Q}_i\eta(x_i) \quad \forall \eta \in \mathcal{V}. \end{array} \right. \tag{5}$$

In the above equations, $M(u)$ is the generalized stress tensor that represents the bending moments in the middle plane of the plate, given by

$$M(u) = -\frac{h^3}{12}\mathbb{C}\nabla\nabla u \, , \tag{6}$$

being $\mathbb{C}$ the fourth-order elastic constitutive tensor. For an isotropic and homogeneous material, this tensor can be written as

$$\mathbb{C} = \frac{E}{1-\nu^2}((1-\nu)\mathbb{I} + \nu \, \mathrm{I}\otimes\mathrm{I}) \, , \tag{7}$$

where I and $\mathbb{I}$ are the second and fourth order identity tensors, respectively, E is the Young modulus and ν the Poisson ratio. The set $\mathcal{U}$ and the space $\mathcal{V}$ are respectively defined as

$$\mathcal{U} := \{\varphi \in H^2(\Omega) : \varphi|_{\Gamma_{D_u}} = \overline{u}, \ \partial_n\varphi|_{\Gamma_{D_\rho}} = \overline{\rho}\} \, , \tag{8}$$

$$\mathcal{V} := \{\varphi \in H^2(\Omega) : \varphi|_{\Gamma_{D_u}} = 0, \ \partial_n\varphi|_{\Gamma_{D_\rho}} = 0\} \, . \tag{9}$$

In addition, h is the plate thickness assumed to be constant everywhere, $\overline{q}$ is a shear load distributed on the boundary Γ_{N_q}, $\overline{m}$ is a moment distributed on the boundary Γ_{N_m} and $\overline{Q}_i$ is a concentrated shear load supported at the points x_i where there are some geometrical singularities, with $i = 1, ..., ns$, and ns the number of such singularities. The deflection field u has to satisfy $u|_{\Gamma_{D_u}} = \overline{u}$ and $\partial_n u|_{\Gamma_{D_\rho}} = \overline{\rho}$, where $\overline{u}$ and $\overline{\rho}$ are a deflection and a rotation respectively prescribed on the boundaries Γ_{D_u} and Γ_{D_ρ}. Furthermore, $\Gamma_D = \overline{\Gamma_{D_u}} \cup \overline{\Gamma_{D_\rho}}$ and $\Gamma_N = \overline{\Gamma_{N_q}} \cup \overline{\Gamma_{N_m}}$ are such that $\Gamma_{D_u} \cap \Gamma_{N_q} = \varnothing$ and $\Gamma_{D_\rho} \cap \Gamma_{N_m} = \varnothing$. See the details in fig. 2.

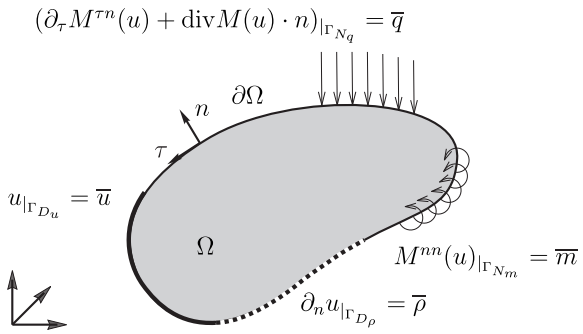

FIGURE 2. The Kirchhoff problem defined in the unperturbed domain.

The strong formulation associated to the variational problem (5) reads:

$$\left\{\begin{array}{l} \text{Find } u, \text{ such that} \\ \begin{array}{rcll} \mathrm{div}(\mathrm{div} M(u)) & = & 0 & \text{in } \Omega\,, \\ M(u) & = & -\frac{h^3}{12}\mathbb{C}\nabla\nabla u & \\ u & = & \overline{u} & \text{on } \Gamma_{D_u}\,, \\ \partial_n u & = & \overline{\rho} & \text{on } \Gamma_{D_\rho}\,, \\ M^{nn}(u) & = & \overline{m} & \text{on } \Gamma_{N_m}\,, \\ \partial_\tau M^{\tau n}(u) + \mathrm{div} M(u)\cdot n & = & \overline{q} & \text{on } \Gamma_{N_q}\,, \\ [\![M^{\tau n}(u(x_i))]\!] & = & \overline{Q}_i & \text{on } x_i \in \Gamma_{N_q}\,, \end{array} \end{array}\right. \tag{10}$$

where $[\![(\cdot)]\!]$ denotes the jump of $(\cdot)$ at the point x_i; and M^{nn} and $M^{\tau n}$ are the components of the stress tensor M in the curvilinear coordinates system defined by the normal and tangential vectors (n, τ) to the boundary $\partial\Omega$.

For an explicit and analytical formula for the topological derivative $\mathcal{T}_\Omega(\widehat{x})$ of the functional (4) associated to the problem (5), when a circular inclusion with constitutive properties $\gamma\mathbb{C}$ is inserted at an arbitrary point $\widehat{x}$, we introduce the following result:

Theorem 2.1. *The topological derivative of the energy shape functional associated to the elastic Kirchhoff plate problem is given by:*

$$\mathcal{T}_\Omega(\widehat{x}) = \mathbb{P}_\gamma M(u(\widehat{x}))\cdot\nabla\nabla u(\widehat{x})\,, \tag{11}$$

where $u(\widehat{x})$ is the solution of the problem (5) evaluated at $\widehat{x}$ and the polarization tensor $\mathbb{P}_\gamma$ is given by the following fourth order isotropic tensor

$$\mathbb{P}_\gamma := \frac{1}{2}\frac{1-\gamma}{1+\gamma\beta}\left(\frac{4\beta}{1-\nu}\mathbb{I} + \alpha\beta\frac{1+3\nu}{1-\nu^2}\frac{1-\gamma}{1+\gamma\alpha}\mathrm{I}\otimes\mathrm{I}\right)\,, \tag{12}$$

where the parameter γ denotes the contrast in the constitutive properties of the elastic medium, I and $\mathbb{I}$ are the identity tensors of second- and fourth-order, respectively, and the parameters α and β depend exclusively on the Poison's ratio of the plate, given by

$$\alpha := \frac{1+\nu}{1-\nu} \quad \textit{and} \quad \beta := \frac{3-\nu}{1+\nu}. \tag{13}$$

Proof. The reader interested in the proof of this result may refer to Amstutz (2010); Novotny et al. (2005). □

Remark 2.2. *Formally, we can take the limit cases $\gamma \to 0$ and $\gamma \to \infty$. For $\gamma \to 0$, the inclusion leads to a void and the transmission condition on the boundary of the inclusion degenerates to homogeneous Neumann boundary condition. In fact, in this case the polarization tensor is given by*

$$\mathbb{P}_0 = \frac{2}{3+\nu}\mathbb{I} + \frac{1+3\nu}{2(1-\nu)(3+\nu)}\mathrm{I}\otimes\mathrm{I}\,. \tag{14}$$

In addition, for $\gamma \to \infty$, the elastic inclusion leads to a rigid one and the polarization tensor is given by

$$\mathbb{P}_\infty = -\frac{2}{1-\nu}\mathbb{I} + \frac{1+3\nu}{2(1-\nu^2)}\mathrm{I}\otimes\mathrm{I}\,. \tag{15}$$

Note that, expression (11) represents the sensitivity of the energy shape functional, associated to the problem (5), to the insertion at an arbitrary point $\widehat{x}$ of a circular disk whose constitutive property is characterized by the contrast parameter γ. The limit cases of this parameter, presented in the above remark, will be used to devise a topological structural optimization algorithm. In order to solve the optimization problem (3), in the next section we present two methods to impose the constraint in the final volume of the domain, by using the previously introduced topological derivative formula.

3. Volume control methods

In this section we propose two methods of volume control, in the context of topological derivative-based structural optimization, to solve the problem stated in (3). The first one is done by means of linear penalization and does not provide direct control over the required volume fraction. In this case, the penalty parameter is the coefficient of a linear term used to control the amount of material to be removed. The second approach is based on the Augmented Lagrangian method which has both, linear and quadratic terms. The coefficient of the quadratic part controls the Lagrange multiplier update of the linear part. Through this last method it is possible to specify the final amount of material in the optimized structure.

For computational purposes, we consider strong and weak materials representing the elastic part and the voids, respectively. We decompose the domain Ω into two disjoint parts Ω^s and Ω^w, representing the strong and weak materials domains, respectively.

3.1. **Linear penalization.**

In this method we re-write the problem (3) as follows

$$\underset{\Omega^s\subset\Omega}{\text{Minimize}}\ \mathcal{F}_\Omega(u) = -\mathcal{J}_\chi(u) + \lambda\,|\Omega^s|\ , \tag{16}$$

where $|\Omega^s|$ is the Lebesgue measure of Ω^s representing the volume of the elastic part and $\lambda > 0$ is a fixed multiplier which imposes a constraint on the volume of elastic material. It means that the shape functional to be minimized is the strain energy stored in the structure with a volume constraint. It should be stressed that the design variable in problem (16) is the topology of the domain Ω^s. Hence, the use of the *exact* topological sensitivity information provided by the topological derivative (11) emerges as a natural alternative in the development of a numerical optimization algorithm to tackle the problem. The topological derivative of the volume constraint in (16) is trivial. Thus, according to (11) and Remark 2.2, the topological derivatives of $\mathcal{F}_\Omega(u)$ are given by:

- For the strong material domain Ω^s:

$$\mathcal{T}^s_\Omega = \mathbb{P}_0 M(u)\cdot\nabla\nabla u - \lambda\ . \tag{17}$$

- For the weak material domain Ω^w:

$$\mathcal{T}^w_\Omega = \mathbb{P}_\infty M(u)\cdot\nabla\nabla u + \lambda\ . \tag{18}$$

3.2. **Augmented lagrangian.**

The Augmented Lagrangian consists in re-writing the optimization problem (3), by introducing a linear term and a quadratic term in order to incorporate the volume constraint. The coefficient of the quadratic part controls the linear part coefficient update in order to reach the desired volume and satisfy the optimality conditions. Using the same idea that we have used in the previous method we state the optimization problem in an equivalent form given by:

$$\underset{\Omega^s\subset\Omega}{\text{Minimize}}\ \mathcal{F}_\Omega(u) = -\mathcal{J}_\chi(u) + \lambda_1 p^+ + \frac{\lambda_2}{2}(p^+)^2\ , \tag{19}$$

where λ_1 and λ_2 are positive parameters and the function p^+ is defined as

$$p^+ := \max\{p, -\frac{\lambda_1}{\lambda_2}\} \ , \tag{20}$$

with function p given by

$$p := \frac{|\Omega^s|}{V} - 1 \ . \tag{21}$$

The topological derivatives of the linear and quadratic terms in (19) are trivial. Considering again the domain decomposition of Ω in Ω^s and Ω^w, and making use of the Remark 2.2, the topological derivatives of (19) are:

- For the strong material domain Ω^s:

$$\mathcal{T}^s_\Omega = \mathbb{P}_0 M(u) \cdot \nabla\nabla u - \max(0, \lambda_1 + \lambda_2 p) \ . \tag{22}$$

- For the weak material domain Ω^w:

$$\mathcal{T}^w_\Omega = \mathbb{P}_\infty M(u) \cdot \nabla\nabla u + \max(0, \lambda_1 + \lambda_2 p) \ . \tag{23}$$

4. Topological derivative based optimization algorithm

The topological derivative-based optimization algorithm devised in Amstutz and Andrä (2006) stands out as a particularly well-suited choice to solve problem (16). The procedure relies on a level-set domain representation Osher and Sethian (1988) and the approximation of the topological optimality conditions by a fixed point iteration. In particular, the algorithm displays a marked ability to produce general topological domain changes uncommon to other methodologies based on a level-set representation and has been successfully applied in Amstutz and Andrä (2006) to topology optimization in the context of two-dimensional elasticity and flow through porous media. For completeness, the algorithm is outlined in the following. For further details we refer to Amstutz and Andrä (2006).

By considering the level-set domain representation, the strong material is characterized by a function $\Psi \in L^2(\Omega)$ such that

$$\Omega^s = \{x \in \Omega, \Psi(x) < 0\} \ , \tag{24}$$

whereas the weak material domain is defined by

$$\Omega^w = \{x \in \Omega, \Psi(x) > 0\} \ . \tag{25}$$

Now, let us consider the topological derivative of the shape functional $\mathcal{F}_\Omega(u)$. According to Amstutz and Andrä (2006), an obvious sufficient condition of local optimality of problem (16) for the class of perturbations consisting of circular inclusions is

$$\mathcal{T}_\Omega(x) > 0 \quad \forall x \in \Omega \ . \tag{26}$$

To devise a level-set-based algorithm whose aim is to produce a topology that satisfies (26) it is convenient to define the function

$$g(x) = \begin{cases} -\mathcal{T}^s_\Omega(x) & \text{if} \quad x \in \Omega^s \\ \mathcal{T}^w_\Omega(x) & \text{if} \quad x \in \Omega^w \end{cases} \ . \tag{27}$$

With the above definition and (24,25) it can be easily established that the sufficient condition (26) is satisfied if the following equivalence relation between g and the level-set function Ψ holds

$$\exists\, \tau > 0 \quad \text{s.t} \quad g = \tau\, \Psi \ , \tag{28}$$

or, equivalently,

$$\theta := \arccos\left[\frac{\langle g, \Psi\rangle_{L^2(\Omega)}}{\|g\|_{L^2(\Omega)}\, \|\Psi\|_{L^2(\Omega)}}\right] = 0 \ , \tag{29}$$

where θ is the angle between the vectors g and Ψ in $L^2(\Omega)$.

Starting from a given level-set function $\Psi_0 \in L^2(\Omega)$ which defines the chosen initial guess for the optimum topology, the algorithm proposed in Amstutz and Andrä (2006) produces a

sequence $(\Psi_i)_{i\in\mathbb{N}}$ of level-set functions that provides successive approximations to the sufficient condition for optimality (28). The sequence satisfies

$$\begin{aligned} &\Psi_0 \in L^2(\Omega)\ , \\ &\Psi_{i+1} \in \mathrm{co}(\Psi_i, g_i) \qquad \forall i \in \mathbb{N}\ , \end{aligned} \tag{30}$$

where $\mathrm{co}(\Psi_i, g_i)$ is the convex hull of $\{\Psi_i, g_i\}$. In the current algorithm the initial guess Ψ_0 is normalized. With $\mathcal{S}$ denoting the unit sphere in $L^2(\Omega)$, the algorithm is explicitly given by

$$\begin{aligned} &\Psi_0 \in \mathcal{S}\ , \\ &\Psi_{i+1} = \frac{1}{\sin\theta_i}\left[\sin((1-\kappa_i)\theta_i)\Psi_i + \sin(\kappa_i\theta_i)\frac{g_i}{\|g_i\|_{L^2(\Omega)}}\right] \qquad \forall i \in \mathbb{N}\ , \end{aligned} \tag{31}$$

where $\kappa_i \in [0,1]$ is a step size determined by a line-search in order to decrease the value of the cost functional $\mathcal{F}_\Omega(u)$ and, by construction of $(31)_2$, we have that $\Psi_{i+1} \in \mathcal{S}\ \forall i \in \mathbb{N}$. The iterative process is stopped when for some iteration the obtained decrease in $\mathcal{F}_\Omega(u)$ is smaller than a given numerical tolerance. If, at this stage, the optimality condition (28,29) is not satisfied to the desired degree of accuracy, i.e. if $\theta_{i+1} > \epsilon_\theta$, where ϵ_θ is a pre-specified convergence tolerance, then a uniform mesh refinement of the structure is carried out and the procedure is continued.

The previously outlined algorithm is complemented by the two volume constraint methods presented in Section 3. In the case of the linear penalization (16), the multiplier λ is kept constant during the whole optimization procedure. Then, no further information is needed for the optimization algorithm. For the Augmented lagrangian formulation (19), the parameter λ_2 in the quadratic term is constant throughout the optimization procedure, and is used to update the parameter λ_1 associated to the linear term. The update rule is:

$$\lambda_1^{i+1} = \max[0, \lambda_1^i + \lambda_2 p_\Omega^i] \quad \forall i \in \mathbb{N}\ , \tag{32}$$

where λ_1^i and p_Ω^i are the values of the parameter λ_1 and the function p_Ω evaluated at the iteration i.

5. Numerical examples

In order to illustrate the difference between the two methods devised to impose the volume constraint, in this section we propose some numerical examples. The *Discrete Kirchhoff Triangle* three node finite element (DKT-9), which is fully detailed in Batoz (1982), is adopted for the discretization of the variational problem (5). The topology is identified by the strong material distribution and the inclusions of weak material are used to mimic the holes. In all examples we consider as initial guess a unit square plate, with Poisson's ratio $\nu = 0.3$ and the product $hE = 1$. The contrast parameter is given by $\gamma = 10^{-3}$. Furthermore, the thick lines that appear on the figures are used to denote clamped ($u = \partial u/\partial n = 0$) boundary conditions. In the remainder part of the boundary, where noting is specified, we consider homogeneous Neumann boundary condition. The results are presented in the following order: For each example we have performed the topology optimization for the linear penalization with a suitable λ which gives us a topology with a 50% of strong material. Then we used different parameters for the augmented lagrangian method $\lambda_2 = \{10, 20, 30\}$ always starting with $\lambda_1 = 0$. We start with a uniform mesh containing 3200 elements and 1681 nodes. Then we perform 3 steps of uniform mesh refinement for each set of parameters. The final uniform mesh contains 204800 finite elements and 103041 nodes. For each example, the black part of the domain represent the strong material and the white part the weak material.

5.1. **Example 1.** In this first example we present a plate subjected to a pair of uniform bending moments, $\overline{m} = 1$ and $\overline{m} = -1$ applied on a region of length 0.5 of the middle of the opposite sides, as shown in fig. 3. We set $\lambda = 3.80$, corresponding to a volume constraint of 50% of hard material. The final topology for each case is presented in fig. 4. The comparison between the volume histories is shown in fig. 5.

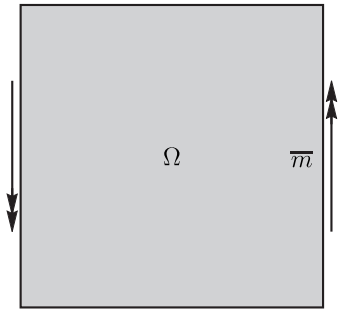

FIGURE 3. Example 1: initial guess.

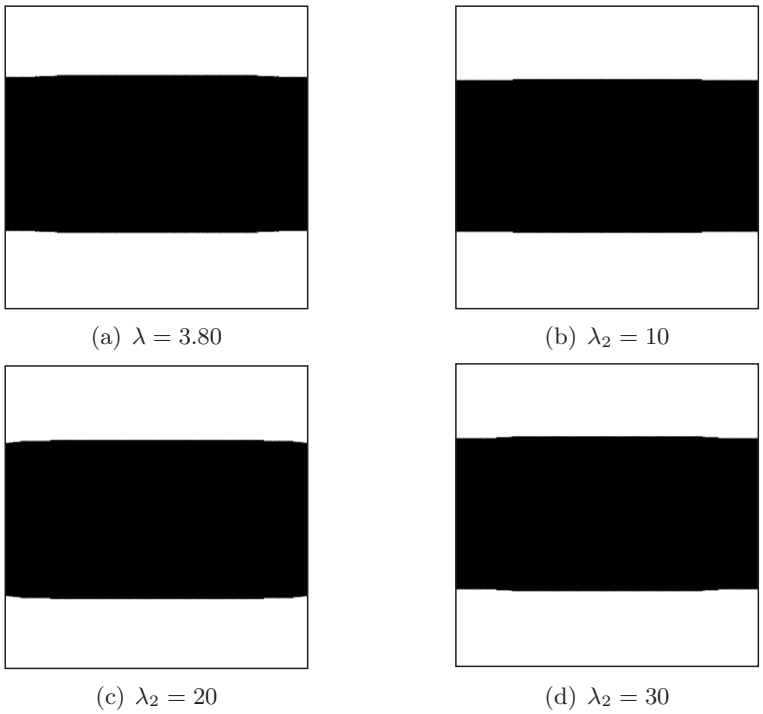

(a) $\lambda = 3.80$ (b) $\lambda_2 = 10$

(c) $\lambda_2 = 20$ (d) $\lambda_2 = 30$

FIGURE 4. Example 1: obtained topologies for the linear penalization (a) and augmented Lagrangian (b)-(d).

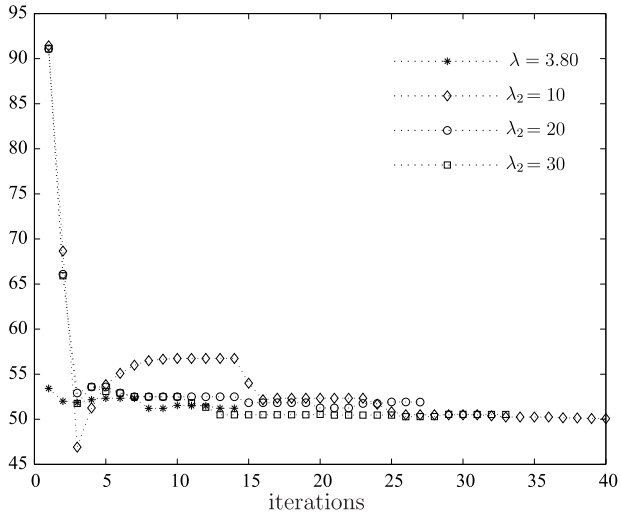

FIGURE 5. Example 1: volume fraction history.

The final topologies shown in Fig. 4 for different choice of parameter λ_2 are qualitatively very close to the one obtained with linear penalization method for $\lambda = 3.80$. The final topology is characterized by a plate connecting the two opposite sides where the uniform bending moments $\overline{m}$ are applied. Therefore, the proposed algorithm seems to be able in finding a possible global minimum for this simple example.

5.2. **Example 2.** In this example we present a plate subjected to three uniform bending moments, $\overline{m} = 1$ applied on a region of length 0.5 (middle) of the right edge and $\overline{m} = -1$ acting on two regions of length 0.25 (top and bottom) of the left edge, as shown in fig. 6. We set $\lambda = 3.88$, corresponding to a volume constraint of 50% of hard material. The final topology for each case is presented in fig. 7. The comparison between the volume histories is shown in fig. 8.

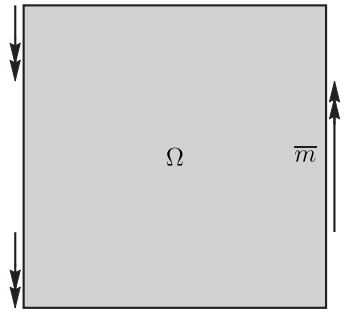

FIGURE 6. Example 2, initial guess.

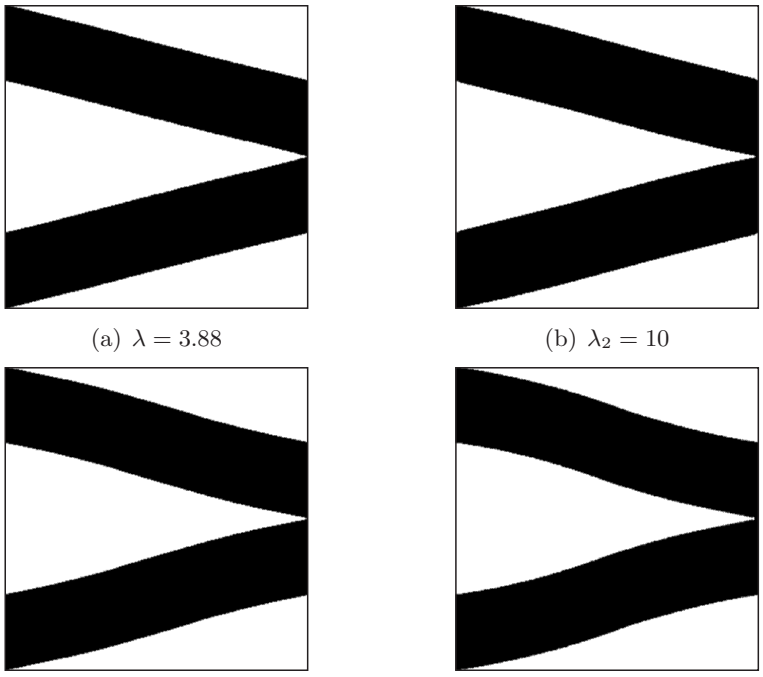

(a) $\lambda = 3.88$ (b) $\lambda_2 = 10$

(c) $\lambda_2 = 20$ (d) $\lambda_2 = 30$

FIGURE 7. Example 2: obtained topologies for the linear penalization (a) and augmented Lagrangian (b)-(d).

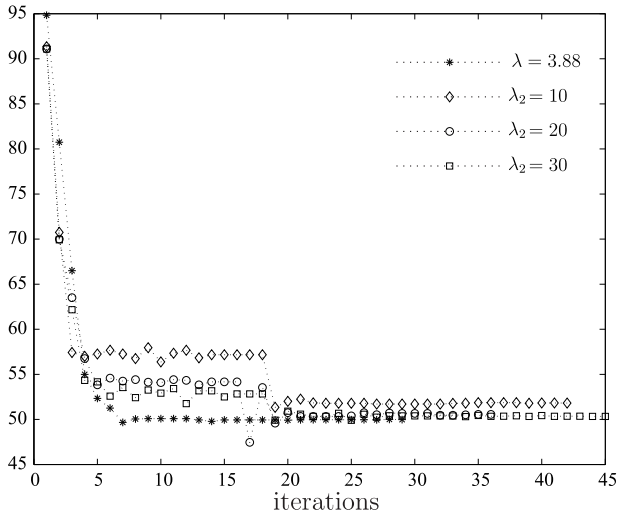

FIGURE 8. Example 2: volume fraction history.

Once again, the final topologies for all parameters λ_2 are qualitatively similar to the result obtained with the linear penalization method for $\lambda = 3.88$, as can be seen in Fig. 7. Here, the optimal topology is characterized by two plates connecting the parts of the boundary where the uniform bending moments $\overline{m}$ are applied. The influence of the parameter λ_2 in the Augmented Lagrangian method is manifested in the shape of the plates. Note that when the parameter λ_2 increases, the plates have a more evident curved shape.

5.3. **Example 3.** In this next example we present a plate subjected to two pairs of uniform bending moments $\overline{m} = 1$ and $\overline{m} = -1$, as shown in fig. 9. The first pair is applied on two regions

of length 0.20 of the top and bottom edges. The second pair is acting on two regions of length 0.20 of the left and right edges. We set $\lambda = 4.40$, corresponding to a volume constraint of 50% of hard material. The final topology for each case is presented in fig. 10(a). The comparison between the volume histories is shown in fig. 11.

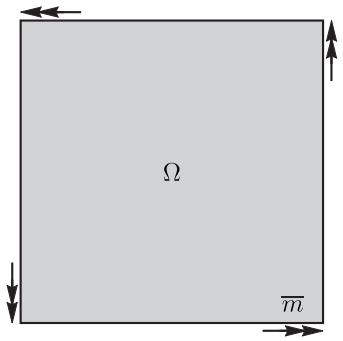

FIGURE 9. Example 3: initial guess.

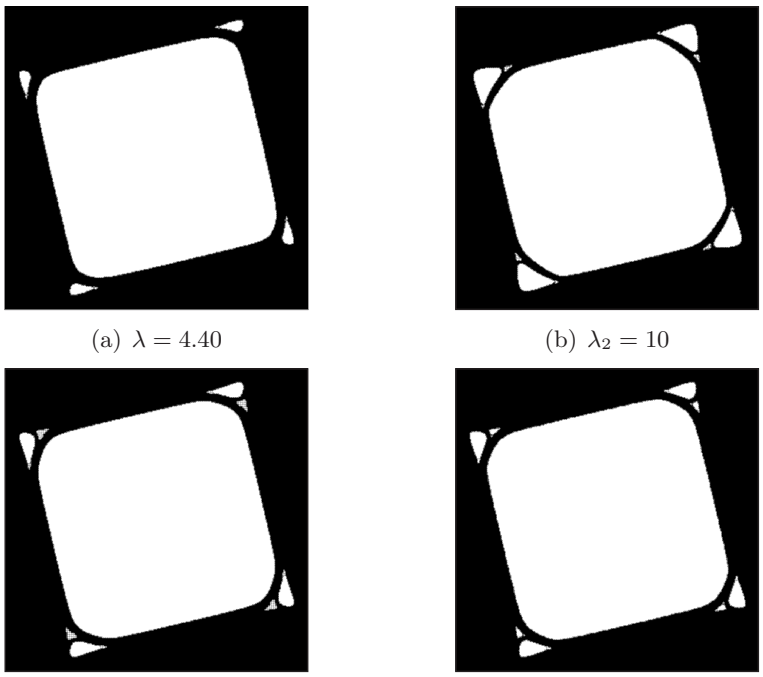

(a) $\lambda = 4.40$ (b) $\lambda_2 = 10$

(c) $\lambda_2 = 20$ (d) $\lambda_2 = 30$

FIGURE 10. Example 3: obtained topologies for the linear penalization (a) and augmented Lagrangian (b)-(d).

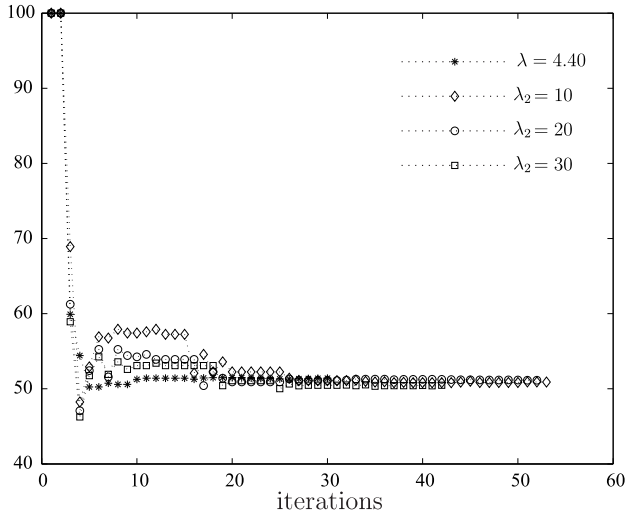

FIGURE 11. Example 3: volume fraction history.

In this example, the optimal topologies change a little bit for all parameter λ_2, if compared with the resulting topology from the linear penalization method for $\lambda = 4.40$, as shown in Fig. 10. However, the topologies obtained with the Augmented Lagrangian method are qualitatively equivalent. We can note a small difference on the size and shape of the holes.

5.4. **Example 4.** In this last example the plate is clamped in two adjacent sides and a concentrated load $\overline{Q}_i = 1$ is applied at the free corner, as illustrated in fig. 12. We set $\lambda = 2.00$, corresponding to a volume constraint of 50% of hard material. The obtained topologies are presented in fig. 13(a). The comparison between the volume histories is shown in fig. 14.

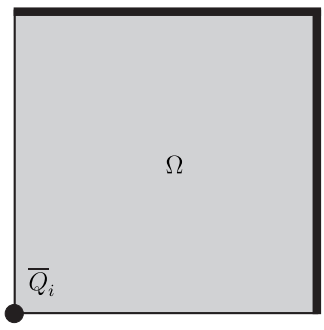

FIGURE 12. Example 4: initial guess

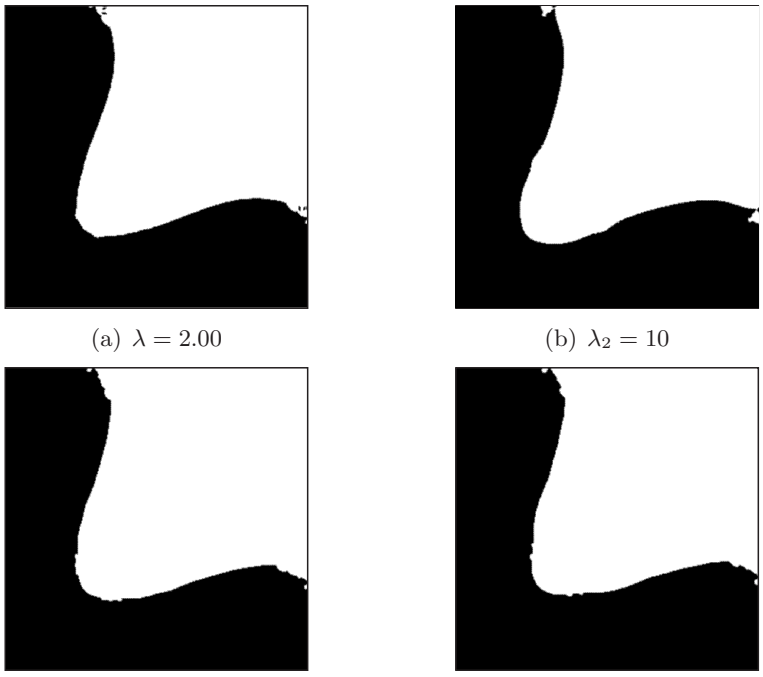

(a) $\lambda = 2.00$ (b) $\lambda_2 = 10$

(c) $\lambda_2 = 20$ (d) $\lambda_2 = 30$

FIGURE 13. Example 4: obtained topologies for the linear penalization (a) and augmented Lagrangian (b)-(d).

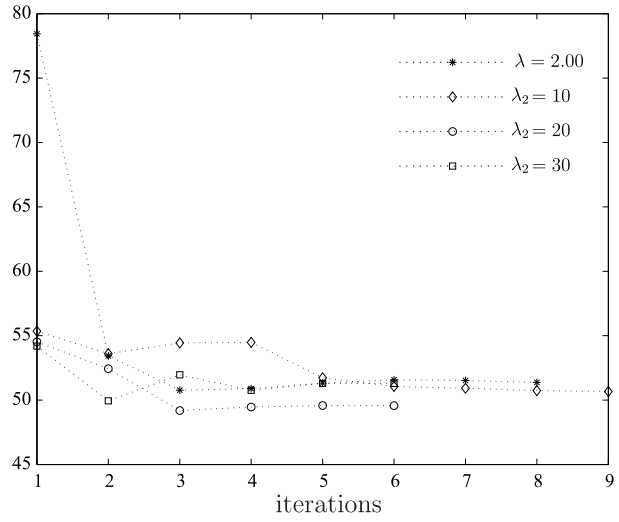

FIGURE 14. Example 4: volume fraction history.

The optimal results are characterized by a L-shaped plate connecting the concentrated load $\overline{Q}_i$ with the clamped boundary. Again, from a qualitative point of view, the final topologies are very close to each other in all cases. Only small differences in the shape can be observed.

6. Conclusions

The topological derivative of the total potential energy associated to the Kirchhoff plate bending problem, considering as singular perturbation the insertion of a small circular inclusion, has been presented. We have formally performed the limit passages when the contrast $\gamma \to 0$ and

$\gamma \to \infty$. For $\gamma \to 0$, the inclusion leads to a void and the transmission condition on the boundary of the inclusion degenerates to homogeneous Neumann boundary condition. In addition, for $\gamma \to \infty$, the elastic inclusion leads to a rigid one. The closed forms of the polarization tensors are identified for both cases. Then, we have compared two methods of volume control in the context of topological derivative-based structural optimization. The first one is done by means of linear penalization. The second approach is based on the Augmented Lagrangian method. In order to present the behavior of both approaches, we have considered the compliance topology optimization of Kirchhoff plates subjected to volume constraint. The associated topological sensitivity has been used in a structural design algorithm based on the topological derivative and a level-set domain representation method. Some numerical experiments have been presented allowing for a comparative analysis between the above two methods of volume control from a qualitative point of view.

In all cases we have observed that the obtained optimal topologies are qualitatively similar. It means that the results obtained with the Augmented Lagrangian method are not strongly affected by the choice of the parameter λ_2, if compared with the topologies obtained with the linear penalization method for a specific choice of the parameter λ. In fact, only small differences in the shape were observed, which probably come out from a lack of sufficient optimality conditions for the compliance topology optimization problem with volume constraint. Related to the computational cost of the optimization procedure, in general the linear penalization method requires less iterations than the Augmented Lagrangian method. However, the linear penalization method does not provide direct control over the required volume fraction. In particular, to acquire a desired volume fraction, the penalty parameter should be determined by hand after some trials (increasing the global cost of the optimization procedure). In contrast, the Augmented Lagrangian method allows to specify the final amount of material in the optimized structure *a priori*. Therefore, this method seems to be more appropriated than the linear penalization method for volume control in topology optimization design.

Finally, we remark that the low computational cost (small number of iterations needed) of the optimization procedure is nothing but a natural consequence of the use of the topological derivative in defining a feasible descent direction for the cost functional, which is based on the exact sensitivity with respect to a singular domain perturbation. In addition, the relative simplicity of the proposed topology optimization algorithm should also be noted. It does not feature post-processing procedures (such as filtering or relaxation) of any kind and only a minimal number of user-defined algorithmic parameters are needed. This is in contrast with existing SIMP-based structural optimization strategies and follows, again, as a natural consequence of the use of the concept of topological derivative.

Acknowledgments

Authors would like to thank Prof. Samuel Amstutz for helpful discussions on this paper. This research was partly supported by CNPq (Brazilian Research Council) and FAPERJ (Research Foundation of the State of Rio de Janeiro), under grants 470597/2010-0 and E-26/102.204/2009, respectively. D.E. Campeão was supported by CNPq. S.M. Giusti was partially supported by CONICET (National Council for Scientific and Technical Research) and PID-UTN (Research and Development Program of the National Technological University) of Argentina under grant N° 1420. The support of these agencies are gratefully acknowledged.

References

Allaire, G., de Gournay, F., Jouve, F., Toader, A. M., 2005. Structural optimization using topological and shape sensitivity via a level set method. Control and Cybernetics 34 (1), 59–80.

Allaire, G., Jouve, F., Van Goethem, N., 2011. Damage and fracture evolution in brittle materials by shape optimization methods. Journal of Computational Physics 230 (12), 5010–5044.

Amstutz, S., 2006. Sensitivity analysis with respect to a local perturbation of the material property. Asymptotic Analysis 49 (1-2), 87–108.

Amstutz, S., 2010. A penalty method for topology optimization subject to a pointwise state constraint. ESAIM: Control, Optimisation and Calculus of Variations 16 (03), 523–544.

Amstutz, S., Andrä, H., 2006. A new algorithm for topology optimization using a level-set method. Journal of Computational Physics 216 (2), 573–588.

Amstutz, S., Giusti, S. M., Novotny, A. A., de Souza Neto, E. A., 2010. Topological derivative for multi-scale linear elasticity models applied to the synthesis of microstructures. International Journal for Numerical Methods in Engineering 84, 733–756.

Amstutz, S., Horchani, I., Masmoudi, M., 2005. Crack detection by the topological gradient method. Control and Cybernetics 34 (1), 81–101.

Amstutz, S., Novotny, A. A., 2010. Topological optimization of structures subject to von Mises stress constraints. Structural and Multidisciplinary Optimization 41 (3), 407–420.

Amstutz, S., Novotny, A. A., de Souza Neto, E. A., 2012. Topological derivative-based topology optimization of structures subject to Drucker-Prager stress constraints. Computer Methods in Applied Mechanics and Engineering 233–236, 123–136.

Batoz, J. L., 1982. An explicit formulation for an efficient triangular plate-bending element. International Journal for Numerical Methods in Engineering 18, 1077–1089.

Bojczuk, D., Mróz, Z., 2009. Topological sensitivity derivative and finite topology modifications: application to optimization of plates in bending. Structural and Multidisciplinary Optimization 39 (1), 1–15.

Giusti, S. M., Novotny, A. A., de Souza Neto, E. A., Feijóo, R. A., 2009. Sensitivity of the macroscopic elasticity tensor to topological microstructural changes. Journal of the Mechanics and Physics of Solids 57 (3), 555–570.

Giusti, S. M., Novotny, A. A., Sokołowski, J., 2010. Topological derivative for steady-state orthotropic heat diffusion problem. Structural and Multidisciplinary Optimization 40 (1), 53–64.

Hintermüller, M., Laurain, A., 2008. Electrical impedance tomography: from topology to shape. Control and Cybernetics 37 (4), 913–933.

Hintermüller, M., Laurain, A., 2009. Multiphase image segmentation and modulation recovery based on shape and topological sensitivity. Journal of Mathematical Imaging and Vision 35, 1–22.

Hintermüller, M., Laurain, A., Novotny, A. A., 2012. Second-order topological expansion for electrical impedance tomography. Advances in Computational Mathematics 36 (2), 235–265.

Larrabide, I., Feijóo, R. A., Novotny, A. A., Taroco, E., 2008. Topological derivative: a tool for image processing. Computers & Structures 86 (13–14), 1386–1403.

Novotny, A. A., Feijóo, R. A., Padra, C., Taroco, E., 2003. Topological sensitivity analysis. Computer Methods in Applied Mechanics and Engineering 192 (7–8), 803–829.

Novotny, A. A., Feijóo, R. A., Padra, C., Taroco, E., 2005. Topological derivative for linear elastic plate bending problems. Control and Cybernetics 34 (1), 339–361.

Novotny, A. A., Sokołowski, J., 2013. Topological derivatives in shape optimization. Interaction of Mechanics and Mathematics. Springer.

Osher, S., Sethian, J. A., 1988. Front propagating with curvature dependent speed: algorithms based on hamilton-jacobi formulations. Journal of Computational Physics 78, 12–49.

Sokołowski, J., Żochowski, A., 1999. On the topological derivative in shape optimization. SIAM Journal on Control and Optimization 37 (4), 1251–1272.

Turevsky, I., Gopalakrishnan, S. H., Suresh, K., 2009. An efficient numerical method for computing the topological sensitivity of arbitrary-shaped features in plate bending. International Journal for Numerical Methods in Engineering 79 (13), 1683–1702.

Van Goethem, N., Novotny, A. A., 2010. Crack nucleation sensitivity analysis. Mathematical Methods in the Applied Sciences 33 (16), 197–1994.

(D.E. Campeão) Coordenação de Matemática Aplicada e Computacional, Laboratório Nacional de Computação Científica LNCC/MCT, Av. Getúlio Vargas 333, Quitandinha, 25651-075, Petrópolis, RJ, Brazil.

E-mail address: dcampeao@lncc.br

(S.M. Giusti) Departamento de Ingeniería Civil, Facultad Regional Córdoba, Universidad Tecnológica Nacional (UTN/FRC - CONICET) Maestro M. López esq. Cruz Roja Argentina, X5016ZAA - Córdoba, Argentina.

E-mail address: sgiusti@civil.frc.utn.edu.ar

(A.A. Novotny) Coordenação de Matemática Aplicada e Computacional, Laboratório Nacional de Computação Científica LNCC/MCT, Av. Getúlio Vargas 333, Quitandinha, 25651-075, Petrópolis, RJ, Brazil.

E-mail address: novotny@lncc.br